Title

Simultaneous intraluminal imaging of tissue autofluorescence and eGFP-labeled cells in engineered vascular grafts inside a bioreactor

Journal

Methods and Applications in Fluorescence, 7(4)

ISSN

2050-6120

Authors

Li, Cai
Alfonso-Garcia, Alba
McMasters, James
et al.

Publication Date

2019

DOI

10.1088/2050-6120/ab4342

Peer reviewed

HHS Public Access

Author manuscript

Methods Appl Fluoresc. Author manuscript; available in PMC 2020 October 07.

Published in final edited form as:

Methods Appl Fluoresc. ; 7(4): 044003. doi:10.1088/2050-6120/ab4342.

Simultaneous intraluminal imaging of tissue autofluorescence and eGFP-labeled cells in engineered vascular grafts inside a bioreactor

Cai Li[1], **Alba Alfonso-Garcia**[2], **James McMasters**[2], **Julien Bec**[2], **Brent Weyers**[2], **Lauren Uyesaka**[2], **Leigh Griffiths**[3], **Alyssa Panitch**[2], **Laura Marcu**[2]

[1]Department of Material Science and Engineering, University of California, Davis, United States of America

[2]Department of Biomedical Engineering, University of California, Davis, United States of America

[3]Department of Cardiovascular Diseases, Mayo Clinic, Rochester, United States of America

Abstract

The growing demand for tissue engineered vascular grafts (TEVG) motivates the development of optimized fabrication and monitoring procedures. Bioreactors which provide physiologically-relevant conditions are important for improving holistic TEVG properties and performance. Herein we describe a fiber-based intraluminal imaging system that allows for *in situ* assessment of vascular materials and re-cellularization processes inside a bioreactor by simultaneous and co-registered measurements of endogenous fluorescence lifetime and exogenous marker fluorescence intensity. The lumen of 6 vascular grafts (~4 mm diameter) were scanned by reciprocally rotating a 41° angle polished multimode optical fiber inside a protective glass tube with outer diameter of 3 mm. Tubular bovine pericardium constructs were recellularized using enhanced Green Fluorescent Protein (eGFP) transfected cells in a custom bioreactor. The imaging system has resolved consistently the cellular autofluorescence from that of tissue matrix *in situ* based on the lifetime fluorescence properties of endogenous molecular species. The location of the re-cellularized area was validated by the eGFP emission. Current results demonstrate the potential of this system as a valuable tool in tissue engineering for *in situ* studies of cell-tissue interactions in cylindrical or other 3-dimensional structures.

Keywords

tissue engineered vascular graft; bioreactor; non-destructive imaging; FLIm; fluorescence

1. Introduction

Vascular grafting is considered an optimal solution for patients who require long-term revascularization [1]. Although autologous arteries or veins are preferred, their availability is limited and their harvest may cause donor site morbidity [2]. As an alternative to autologous

lmarcu@ucdavis.edu.

grafts, synthetic materials have demonstrated satisfying results for large diameter arteries, but suffered from poor patency rates when used in small diameter vessels [2, 3]. Given the limitations of autologous and synthetic vascular grafts, tissue engineered vascular grafts (TEVG) with the ability to grow, remodel and repair, are under consideration for treatments of cardiovascular disease [2,4].

The increased demand for developing robust, physiologically-relevant TEVGs motivates new methods for optimizing fabrication procedures and monitoring maturation which ensure adequate biochemical and biomechanical properties. These procedures include choosing fabrication materials (scaffolds and cells) and characterizing their properties, as well as building protocols for scaffold conditioning (i.e. decellularization) and recellularization with host-derived cells [2]. Previous studies have demonstrated the value of culturing TEVG in bioreactors that mimic physiological flow conditions including improving matrix biochemical composition [5], enhancing TEVGs' mechanical properties [6] and strengthening endothelial cell adhesion [7]. In addition, using bioreactors provides an opportunity for studying biomechanics of tissue growth and remodeling processes under controlled environmental stimuli.

Conventional methods such as histology or mechanical tests to assess tissue properties as they grow, share a major shortcoming: they all require tissues to be moved out of the bioreactor and processed irreversibly [8, 9], resulting in sample destruction, making the study costly and time-consuming. Therefore, there is an unmet need for non-destructive alternative methods to quantify tissue growth parameters *in situ*. Achieving this goal is further complicated by three-dimensional geometries such as tubular TEVGs with cellular activity in the luminal surface.

Non-destructive evaluation of TEVG morphology has previously been implemented with magnetic resonance imaging (MRI) by Mertens *et al* [10]. For that work, ultrasmall superparamagnetic iron oxide (USPIO) nanoparticles were incorporated into the polymer matrix and further cultured in the bioreactor. In addition, Whited *et al* utilized fluorescence imaging for tracking endotheliazation of the luminal side of TEVG cultured inside a bioreactor. Their strategy consisted of embedding two micro capillary channels for fiber optic excitation of the GFP-labeled endothelial cells [11]. Despite the success of these methods to accomplish longitudinal monitoring of tissue development, TEVGs were heavily modified for imaging purposes, increasing their complexity in detriment of their potential for further development [12]. Label-free imaging techniques can circumvent some of these pitfalls and reduce the complexity of sample preparation. For example, the potential of intravascular optical coherence tomography (OCT) for imaging TEVGs inside bioreactors was reported with remarkable results in resolving wall thickness and scaffold degradation [13]. Moreover, a recently developed micro optical coherence tomography (μOCT) technique has shown potential to image the endothelial cell layer in coronary arteries [14]. While OCT excels at resolving these structural features in tissues, it fails to provide functional information associated with biochemical changes of the TEVGs.

Endogenous fluorescence, however, reports on biochemical features of tissue samples. Structural proteins (e.g. collagen and elastin) fluoresce under ultraviolet (UV) excitation.

Their fluorescence properties can be correlated with tissue biochemical and biomechanical properties [15, 16]. Cells also express endogenous fluorescence under UV light that excites nicotinamide adenine dinucleotide (NADH) and flavin adenine dinucleotide (FAD) [17, 18], co-factors in cellular metabolism [19]. A mature TEVG consists of a matrix mainly formed by collagen and elastin that will generate strong endogenous fluorescence signals [1] and embedded cells that will moderately contribute to the overall autofluorescence. Therefore, it is possible to non-destructively characterize the tissue and cellular properties by measuring endogenous fluorescence without any prior modification of the sample. A caveat to this approach is posed by the significant overlap between the emission spectra of cells with that of the main structural proteins [20], which challenges the study of cellular activity on tissue. A previous study from our group demonstrated the possibility of resolving seeded cells from a collagenous matrix measuring endogenous fluorescence lifetime [21]. The imaging conditions in the previous fluorescence lifetime study were favorable: the flat sample geometry enables a tight control of the probe-to-sample distance and validation of cell presence was easily performed by conventional fluorescence microscopy. However, imaging inside a bioreactor complicates the geometry of the sample (i.e. tubular shape) and the probe-to-sample distance becomes more difficult to control. Additionally, using fluorescence microscopy for validation purposes would require cutting the sample open to expose the lumen, interrupting further development. For these reasons, it becomes necessary to incorporate a non-destructive validation method to demonstrate the system's ability for imaging luminal cell presence inside the bioreactor. Thus, we have incorporated an intensity-based exogenous fluorescence imaging system to the FLIm instrument that acquires specific fluorescence from cell markers in parallel and co-registered to the endogenous fluorescence lifetime images.

In a recent study, we described a fiber based dual-modality instrument that combines a multispectral fluorescence lifetime imaging (FLIm) module that allows for measurements of tissue autofluorescence with a steady-state module tailored to imaging of cells expressing enhanced green fluorescence protein (eGFP) [22]. The current study is focused on adapting this instrument to intraluminal imaging in a bioreactor and on demonstrating its sensitivity for cellular fluorescence. Here we describe the integration of the dual-modality system with a custom-built bioreactor for TEVGs growing by adapting a fiberoptic probe for side-viewing illumination/collection and intraluminal imaging via reciprocal scanning. The instrument accuracy to time-resolved fluorescence was demonstrated by measuring fluorescent dyes with distinct lifetime. The spatial resolution of the fiberoptic scanning probe was estimated by imaging a stent phantom. Finally, the sensitivity of the integrated instrument was evaluated by imaging tissue samples in the bioreactor and resolving eGFP-human mesencymal stem cells fluorescence from antigen-removed bovine pericardium tissue matrix. This system could be easily adapted for other reported TEVG bioreactors [5, 6] due to the flexibility of the optical fiber probe.

2. Methods and materials

2.1. Bioreactor assembly

A custom bioreactor was designed and fabricated. Figure 1 depicts the bioreactor composed of a custom made graft chamber, a media reservoir, and a pulsatile pump. Figure 1(a) shows a schematic of the bioreactor with a render of the graft chamber. The chamber consisted of two pairs of 3D printed polysulfone flanges (Protolabs, USA) connected by two blunt-tip stainless steel dispensing needles (6710A41, McMaster-Carr, USA) with distal end sealed by heat curing epoxy (353 ND-T, Epoxy Technology, Inc. USA). The inner and outer parts of the polysulfone flanges were attached with two sets of stainless steel socket cap screws and sealed inside an O.D. 25 mm Pyrex glass tube by two 1.5 mm wide, I.D. 17 mm chemical resistance O-rings (1185N39, McMaster-Carr, USA). Stainless steel straight connectors (SBP-140-SS, Pneumadyne, Inc. USA) were used to hold the vascular grafts inside the chamber. All the connectors and dispensing needles were further sealed with chemical resistance O-rings (McMaster-Carr, USA). The flow circuit included a media reservoir consisting of a 100 ml Pyrex media bottle. The cap of the bottle was laser cut and replaced with a thin polydimethylsiloxane (PDMS) cap that allows for gas exchange to maintain adequate oxygen, CO_2, and humidity levels inside the bioreactor. Barbed connectors and silicon tubing were used to circulate media between the reservoir and the graft chamber. The pulsatile flow was generated by attaching the silicon tubing to a 4 channel peristaltic pump (FH100M, Thermo Scientific, USA) that pumps the media from reservoir to the graft chamber. A Y connector was used to split the flow: one went through the intraluminal surface of the vascular graft while the other entered the chamber through the dispensing needles and circulated outside the graft (figure 1(b)). The two flows were combined by another Y connector and guided back to the media reservoir, completing the circuit. The entire setup was placed inside an incubator at 5% CO_2 and 37.0 °C (figure 1(b)). All the parts of the graft chamber, the reservoir, and the tubing were autoclaved prior to any use.

2.2. Endogenous and exogenous fluorescence imaging system

Figure 2(a) shows a schematic of the dual-modality endogenous and exogenous (eGFP) fluorescence system that was included in our recent work. Briefly, the FLIm module allowing for measurements of tissue endogenous fluorescence consisted of a 355 nm excitation pulsed laser generated by third harmonic generation of a passive Q-switched Ni:YAG laser (STV-02E, TEEM photonics, France). The emitted fluorescence was collected and parsed by a custom wavelength selection module (WSM) to four different spectral bands (spectral bands: SB1: 381–399 nm, SB2: 415–440 nm, SB3: 532–553 nm, SB4: 572–642 nm). After the WSM, four delay fibers of different length (1, 10, 19 and 28 m) sent light from each spectral band sequentially into a single microchannel plate photomultiplier tube (MCP PMT, R3809U-50, Hamamatsu, Japan) and the electronic signals were further amplified and sampled by a high-speed digitizer running at 12.5 GS/s (NI PXIe-5185, National Instruments, USA).

Because the excitation pulse of the FLIm module was generated at 1 kHz and the fluorescence signal always decays in the order of 1–10 ns, the duty circle of this module is less than 0.1%. This generates a big silent time window, creating an opportunity to inter-

leave other imaging modalities in the system, for example, a module for detection of exogenous probes fluorescence emission. A reflective optical chopper wheel (ROCW, MC1F10A, Thorlabs, Inc. USA) was placed in the optical path and synchronized with the FLIm excitation (UV pulsed laser) such that it transmitts the UV pulses and the endogenous fluorescence for FLIm, and it reflected the exogenous excitation and emission to the steady-state fluorescence imaging system. The eGFP fluorescence was induced by a continuous wave (cw) laser centered at 440 nm (TECBL-50G-440-USB, World Star Tech, Canada) and detected by a photoreceiver (2001-FS, Newport, USA) with a band pass filter (510/84 nm) in front. In this way, the eGFP fluorescence and endogenous FLIm data are co-registered and synchronously measured. Different from the previous report, we increased the sensitivity of our instrument by extracting the exogenous emission signal at the carrier frequency of 1 kHz from the photoreceiver output with a lock-in amplifier (SR530, Stanford Research Systems, USA), using the output from the ROCW controller (MC1000, Thorlabs, Inc. USA) as reference. The magnitude output of the lock-in amplifier was then sampled by another digitizer (NI PXIe-5114, National Instruments, USA) running at 20 kS/s.

In order to image the luminal surface of vascular grafts inside the bioreactor, a 2 mm I.D. and 3 mm O. D. borosilicate glass tube with one end sealed was inserted all through the graft chamber providing a transparent imaging channel (figure 1(b)). A side-viewing optical fiber probe was then inserted into the glass tube for imaging. The scanning was performed by reciprocally rotating the optical fiber probe with a Nema 8 hollow shaft stepper motor (8HY0001-7SK, Jinan Link, China) and pull-backed by a uni-axial stage (Parker, USA). Figure 2(c) shows the distal end of the side viewing optical fiber probe, a 400 μm multimode fiber (FVP400440480, Polymicro Technologies, USA) polished at 41° (the angle between the fiber axis and the polishing surface) and glued to a 19 Gauge hyperdermic tube by heat curing epoxy (320, Epoxy Technology, Inc. USA).

2.3. Phantom preparation and measurements

The dye phantom was made from four small quartz capillaries with different fluorescent dyes inside and attached around the borosilicate glass tube that was used for imaging in the bioreactor (figure 3(a)). The four dyes included two fluorescent dyes: 5 mM Fluorescein and 100 μM Rhodamine 6G, both dissolved in ethanol, as well as two tissue endogenous fluorophores: 500 μM NADH (Sigma, USA) on 0.1 M MOPS buffer (Alfa Aesar, USA), and 2 mg/ml FAD (Sigma, USA) in pure water. The dye solutions were injected into small capillaries sealed on both ends and fixed around the borosilicate glass tube. During imaging, a 2 cm section was imaged with the system by inserting the optical fiber probe through the glass imaging tube. Scanning was performed with a step-size of 2° in the circumferential direction and 200 μm in the axial direction.

The second phantom was made of fluorescent Poly (methylmethacrylate) (PMMA) with a drug-eluting stent (wire diameter of around 40 μm; AXUS Liberté Atom Paclitaxel-Eluting Coronary Stent System, Boston Scientific, USA) placed inside to provide structural features, and it was used for estimating the resolution of the imaging system (figure 3(b)). The borosilicate glass tube was inserted inside the phantom to image the stent with 2° and 200 μm step-size.

2.4. Tissue and cell preparation

To demonstrate the system's potential for imaging in bioreactor-based applications, we tested the system's ability to detect human mesenchymal stem cells (hMSC) seeded on the luminal serous surface of antigen removed bovine pericardium (AR-BP) prepared as previously described [23, 24]. Figure 4(a) shows the procedure of tissue sample preparation. AR-BP was locally seeded with eGFP-hMSC as detailed elsewhere [21]. Six AR-BP pieces of 1.5 cm wide by 4 cm long were washed in cell culture media consisted of DMEM high glucose, 1% (vol/vol) penicillin-streptomycin, 1%(vol/vol) L-glutamine 200 mM (Hyclone Laboratories, South Logan, UT, USA), and 20% (vol/vol) FBS (Atlanta Biologicals,Lawrenceville, GA, USA) overnight on a shaker at 4 °C. 70 μl with 40,000 eGFP-hMSC were seeded using a glass cylinder (Pyrex cloning cylinder, inner diameter 4 mm) onto the serous side of AR-BP. After overnight incubation the cylinders where removed and cell attachment was confirmed by fluorescence microscopy (eGFP filter set Ex. 470/40 nm, Em. 525/50 nm, Dichoric mirror at 495 nm; BZ-X710, Keyance Itasca, IL, USA). Full scaffold images were taken with a Plan Fluor 4x/0.13NA objective lens (Nikon, Japan). The scaffolds were subsequently sutured with a simple continuous 6-0 proline suture joining the two 4 cm long sides to one another to form a tubular shape and onto the bioreactor graft chambers for imaging. The imaging was performed by inserting the glass tube first and then the side view fiber probe which was moved with a step size of 5° in the circumferential direction and 200 μm in the axial direction.

2.5. Image processing and statistics

The fluorescence lifetime was calculated based on previous reported Laguerre basis deconvolution method [25]. All the endogenous fluorescence lifetime images and exogenous eGFP fluorescence intensity images were denoised using box filters for better display. The statistical analysis of lifetime difference between cell and tissue regions was performed comparing pixels within these two regions of the lifetime images for all six samples. A split violin plot was used to display the lifetime distribution of these two regions and a Student's t-test was used to testify their significant difference. The aforementioned processes were performed in Matlab 2018a and R.

3. Results

3.1. Instrument imaging performance

The two custom phantoms used for the evaluation of dual-modality system performance are depicted in figures 3(a) and (b). Figure 3(c) shows the intensity weighted fluorescence lifetime images in SB3 (532–553 nm) which exhibits fluorescence from all chosen fluorophores. The mean ± standard deviation fluorescence lifetime in SB3 were calculated to be: 0.61 ± 0.06 ns for NADH, 2.72 ± 0.06 ns for FAD, 3.82 ± 0.04 ns for Rhodamine 6G and 3.49 ± 0.09 ns for Fluorescein, consistent with literature values [17, 26, 27]. Figure 3(d) shows the normalized eGFP fluorescence intensity image acquired within the same measurement, where fluorescein was visualized easily.

Figure 3(e) shows the SB3 normalized intensity image of the stent phantom in gray scale. The fluorescence origniates from the main body of the stent phantom made of PMMA with a

strong fluorescence in SB3 that serves as background for visualizing the stent itself. From the image, it is easy to resolve the fine structure of the stent (in black) that has an average diameter of 40 μm measured under the microscope.

3.2. Imaging vascular grafts in the bioreactor

Figure 4(b) shows the eGFP fluorescence intensity image of a representative flat hMSC seeded AR-BP before suturing, acquired by conventional fluorescence microscopy. Cells localized in two circular regions. Figure 4(c) shows the eGFP exogenous fluorescence image of the luminal surface same sample sutured on the bioreactor acquired using the dual-modality fiberoptic system. The two circular cellularized regions were successfully detected. The image also shows that part of the bottom cellularized area was compromised likely during sample preparation. Figure 4(d) shows the corresponding SB3 (532–553 nm) endogenous fluorescence lifetime image of sample, which was acquired in parallel with figure 4(c). There is a clear contrast between the cell seeded region with a lifetime of 4.88 ± 0.08 ns and the non-cell seeded region with a lifetime of 5.14 ± 0.09 ns. The split violin plot (figure 4(e)) shows the SB3 lifetime distributions of cell and tissue regions for all six samples, which all followed an equivalent trend. The fluorescence lifetime of cellularized areas decreases an average of 0.33 ± 0.21 ns with respect to the acellular scaffold ($p < 0.001$). The variance is attributed intrinsic sample variations. The trend of lower lifetime for cell seeded region was found consistent with previous studies [21].

4. Discussion

In this study, we present a fluorescence imaging system that seamlessly couples with a bioreactor for intraluminal imaging of developing TEVG. We demonstrated the system's ability to simultaneously acquire fluorescence lifetime images with co-registered exogenous fluorescence intensity images of tubular phantoms with enough resolution to detect tissue level contrast (figure 3). The FLIm module has the sensitivity to resolve cellular fluorescence from natural matrix fluorescence background non-destructively (figures 4(d) and (e)). Our previous studies have shown the capabilities of this FLIm system to monitor tissue level property changes using all four spectral band-widths (SB) [16, 21, 28]. After demonstrating the system capability for capturing weak cellular fluorescence, we anticipate that the integration with the bioreactor will enable monitoring properties of maturing TEVG inside the bioreactor non-destructively. Different from previously reported methods, which either modified graft fabrication procedures in favor of imaging or can only provide structural information [10, 11, 13], our system can provide biochemical information about the composition of tissue as well as cellular activity without compromising the TEVG fabrication processes inside a bioreactor. To validate endogenous FLIm results, the current exogenous fluorescence modality is configured to detect eGFP (figure 4(c)), further validated with conventional fluorescence microscopy of the flat sample prior to suturing (figure 4(b)). It should be noted that due to the reflective optical chopper wheel the two modalities (i.e. endogenous FLIm vs exogenous cw fluorescence) can be decoupled. Thus, it is easy to adapt the exogenous fluorescence modality to any fluorescence label of interest, making it a suitable tool for either validating findings from endogenous fluorescence images or providing extra information related to cell-tissue interactions.

As opposed to conventional intravascular imaging that requires fast scanning speeds typically achieved by using a fiber rotary joint [26], imaging inside a bioreactor is more tolerant to slow scanning speed. Therefore, helical scanning was performed by reciprocally rotating the optical fiber bypassing a fiber rotary joint that introduces extra transmission losses [29], compromising detection of cellular fluorescence. For this iteration of the instrument, we focused on increasing the sensitivity by capitalizing on high averaging, namely 64 waveforms for each pixel, which resulted in an increased signal to noise ratio (SNR) but also an increase of data acquisition (DAQ) time. The DAQ time includes data acquisition, pulling data from digitizer, PMT gain controlling, real time waveform display, and saving for a single pixel. The fastest performance of the current instrument is achieved by running the UV excitation laser at its maximum repetition rate, but this time is increased by synchronizing the reflective optical chopper wheel (ROCW) rotation to the UV excitation laser pulse. Using a 10 slot ROCW with the chopping frequency at 1 kHz, the present DAQ time was around 80 ms and the scanning speed was 4 rpm. A 20 mm vascular graft was fully covered in 20 min with an axial step size of 200 μm and a lateral step angle of 5°. In future work, the scanning speed can be improved by burst pulsing the UV excitation laser to asynchronously acquire endogenous FLIm and exogenous fluorescence intensity images or directly increasing the chopping frequency to match the laser maximum repetition rate using a ROCW with more slots. Another significant change may involve more sensitive detectors in order to reduce the number of waveforms averaging for each pixel. Nonetheless, the ultimate application for this instrument was using the endogenous fluorescence lifetime modality to monitor vascular graft maturation processes, so it is expected that the imaging speed will not be limited by the ROCW.

Another critical aspect of the current instrument is the side viewing optical fiber probe. The current probe was a 400 μm core multimode optical fiber with its distal end polished to 41° without reflective coating. By inserting the optical probe to a transparent glass imaging tube that provides an air interface, the light reflection is realized by total internal reflection on the angled polished surface. Using this probe, the output average laser power were 0.70 mW for the endogenous fluorescence modality (355 nm pulsed laser, 1 kHz repetition rate) and 0.70 mW for exogenous fluorescence modality (440 nm cw laser modulated by ROCW at 1 kHz with 50% duty circle). Comparing with an enface viewing optical fiber of the same characteristics, the angled surface introduced a loss of −0.81 dB, likely due to light leaking through the angled polished surface by refraction. In addition, although the probe resolution was adequately suitable for this tissue level study as demonstrated with the stent phantom (figures 3(d)-(e)), it was not comparable to those using distal optics like GRIN lens or free-form optics [30, 31] because of beam divergence. However, with no component added at the distal end, the current probe had the fluorescence background as clean as a bare fiber at UV light excitation and less throughput loss at the interfaces. This is important for high sensitivity applications such as the detection of weak cellular fluorescence in tissue. In order to improve the optical performance without reducing system sensitivity, future work will explore the possibility of fusion splicing a silica based ball lens or free form optics to the distal end of this multimode fiber [32].

5. Conclusion

We report the development of an endogneous FLIm and exogenous cw fluorescence imaging system integrated with a custom bioreactor for intraluminal imaging of tissue engineered vascular grafts (TEVG). This system permits the scanning of TEVG luminal surfaces in their maturing environment (inside a bioreactor), acquires time-resolved fluorescence images from tissue endogenous fluorophores for sensitive detection of biochemical and structural features, and enables co-registration of each measurement with fluorescence derived from exogenous molecular probes (e.g. eGFP). Benefiting from its non-destructive *in situ* nature, this dual-modality system provides a valuable research tool for tissue engineering studies of cell-tissue interactions in three dimensional culture conditions, such as exploring mechanisms of tissue remodelling and recellurization, as well as optimizing protocols for fabricating vascular grafts.

Acknowledgments

The work is supported by National Institute of Health Grant. R01HL121068 and R03EB025565. The authors have declared that no conflicting interests exist.

References

[1]. Pashneh-Tala S, MacNeil S and Claeyssens F 2015 The tissue-engineered vascular graft-past, present, and future Tissue Eng. Part B Rev 22 68–100 [PubMed: 26447530]

[2]. Masden DL, Seruya M and Higgins JP 2012 A systematic review of the outcomes of distal upper extremity bypass surgery with arterial and venous conduits J. Hand. Surg. Am 37 2362–7 [PubMed: 23044478]

[3]. Hehrlein FW, Schlepper M, Loskot F, Scheld HH, Walter PC and Mulch J 1984 The use of expanded polytetrafluoroethylene (ptfe) grafts for myocardial revascularization The Journal of Cardiovascular Surgery 25 549–53 [PubMed: 6334688]

[4]. Lutz B, Reeps C, Biro G, Knappich C, Zimmermann A and Eckstein H-H 2017 Bovine pericardium as new technical option for *in situ* reconstruction of aortic graft infection Annals of Vascular Surgery 41 118–26 [PubMed: 27903471]

[5]. Song L, Zhou Q, Duan P, Guo P, Li D, Xu Y, Li S, Luo F and Zhang Z 2012 Successful development of small diameter tissue-engineering vascular vessels by our novel integrally designed pulsatile perfusion-based bioreactor PLoS One 7 e42569 [PubMed: 22880036]

[6]. Hahn M S, McHale M K, Wang E, Schmedlen R H and West J L 2007 Physiologic pulsatile flow bioreactor conditioning of poly (ethylene glycol)-based tissue engineered vascular grafts Ann. Biomed. Eng 35 190–200 [PubMed: 17180465]

[7]. Ott M J and Ballermann B J 1995 Shear stress-conditioned, endothelial cell-seeded vascular grafts—improved cell adherence in response to in-vitro shear-stress Surgery 117 334–9 [PubMed: 7878541]

[8]. Lattouf R, Younes R, Lutomski D, Naaman N, Godeau G, Senni K and Changotade S 2014 Picrosirius red staining: a useful tool to appraise collagen networks in normal and pathological tissues Journal of Histochemistry & Cytochemistry 62 751–8 [PubMed: 25023614]

[9]. Claramunt R, Alvarez-Ayuso L, Garcia-Paez JM, Ros A and Casado M C 2013 Changes in the mechanical properties of chemically treated bovine pericardium after a short uniaxial cyclic test Artif. Organs 37 183–8 [PubMed: 23043423]

[10]. Mertens ME et al. 2015 Uspio-labeled textile materials for non-invasive mr imaging of tissue-engineered vascular grafts Biomaterials 39 155–63 [PubMed: 25465443]

[11]. Whited BM. et al. 2013; Dynamic, nondestructive imaging of a bioengineered vascular graft endothelium. PLoS One. 8:e61275. [PubMed: 23585885]

[12]. Appel AA, Anastasio MA, Larson JC and Brey EM 2013 Imaging challenges in biomaterials and tissue engineering Biomaterials 34 6615–30 [PubMed: 23768903]

[13]. Chen WW, Yang JQ, Liao WJ, Zhou JH, Zheng JY, Wu YH, Li DF and Lin ZY 2017 In vitro remodeling and structural characterization of degradable polymer scaffold-based tissue-engineered vascular grafts using optical coherence tomography Cell and Tissue Research 370 417–26 [PubMed: 28887711]

[14]. Nishimiya K, Yin BW, Piao ZL, Osman H, Ryu J, Leung HM, Sharma G, Gardecki J and Tearney G 2018 High-definition micro-optical coherence tomography for endothelial cell visualization in the coronary arteries J. Am. College Cardiol 72 B28–9

[15]. Lewis W, Padilla-Martinez JP, Ortega-Martinez A and Franco W 2016 Changes in endogenous uv fluorescence and biomechanical stiffness of bovine articular cartilage after collagenase digestion are strongly correlated J. Biophotonics 10 1018–1025 [PubMed: 27714971]

[16]. Li C, Shklover J, Parvizi M, Sherlock BE, Alfonso Garcia A, Haudenschild AK, Griffiths LG and Marcu L 2018 Label-free assessment of collagenase digestion on bovine pericardium properties by fluorescence lifetime imaging Ann. Biomed. Eng 46 1870–1881 [PubMed: 30003502]

[17]. Wahl P, Auchet JC, Visser AJWG and Muller F 1974 Time resolved fluorescence of flavin adenine-dinucleotide FEBS Lett. 44 67–70 [PubMed: 4855213]

[18]. Blacker TS, Mann ZF, Gale JE, Ziegler M, Bain AJ, Szabadkai G and Duchen MR 2014 Separating nadh and nadph fluorescence in live cells and tissues using flim Nat. Commun 5 3936 [PubMed: 24874098]

[19]. Wu YC, Zheng W and Qu JNY 2006 Sensing cell metabolism by time-resolved autofluorescence Opt. Lett 31 3122–4 [PubMed: 17041655]

[20]. Croce AC and Bottiroli G 2014 Autofluorescence spectroscopy and imaging: a tool for biomedical research and diagnosis Eur. J. Histochem 58 320–37

[21]. Alfonso-Garcia A, Shklover J, Sherlock BE, Panitch A, Griffiths LG and Marcu L 2018 Fiber-based fluorescence lifetime imaging of recellularization processes on vascular tissue constructs J. Biophotonics 11 e201700391 [PubMed: 29781171]

[22]. Alfonso-Garcia A, Li C, Bec J, Yankelevich D and Sherlock B 2019 Fiber-based platform for synchronous imaging of endogenous and exogenous fluorescence of biological tissue Opt. Lett 44 3350–3353 [PubMed: 31259958]

[23]. Wong ML, Wong JL, Athanasiou KA and Griffiths LG 2013 Stepwise Solubilization-Based Antigen Removal for Xenogeneic Scaffold Generation in Tissue Engineering 9 6492–6501

[24]. Liu ZZ, Wong ML and Griffiths LG 2016 Effect of bovine pericardial extracellular matrix scaffold niche on seeded human mesenchymal stem cell function Sci. Rep 6 37089 [PubMed: 27845391]

[25]. Liu J, Sun Y, Qi J and Marcu L 2012 A novel method for fast and robust estimation of fluorescence decay dynamics using constrained least-squares deconvolution with laguerre expansion Phys. Med. Biol 57 843–65 [PubMed: 22290334]

[26]. Lakowicz JR, Szmacinski H, Nowaczyk K and Johnson ML 1992 Fluorescence lifetime imaging of free and protein-bound nadh Proc. of the National Academy of Sciences of the United States of America 89 1271–5

[27]. Magde D, Rojas GE and Seybold PG 1999 Solvent dependence of the fluorescence lifetimes of xanthene dyes Photochem. Photobiol 70 737–44

[28]. Sherlock BE, Harvestine JN, Mitra D, Haudenschild A, Hu J, Athanasiou KA, Leach JK and Marcu L 2018 Nondestructive assessment of collagen hydrogel cross-linking using time-resolved autofluorescence imaging J. Biomed. Opt 23 036004

[29]. Ma DL, Bec J, Yankelevich DR, Gorpas D, Fatakdawala H and Marcu L 2014 Rotational multispectral fluorescence lifetime imaging and intravascular ultrasound: bimodal system for intravascular applications J. Biomed. Opt 19 066004 [PubMed: 24898604]

[30]. Scolaro L, Lorenser D, Madore WJ, Kirk RW, Kramer AS, Yeoh GC, Godbout N, Sampson DD, Boudoux C and McLaughlin RA 2015 Molecular imaging needles: dual-modality optical coherence tomography and fluorescence imaging of labeled antibodies deep in tissue Biomed. Opt. Express 6 1767–81 [PubMed: 26137379]

[31]. Li JW. et al. 2018; Two-photon polymerisation 3d printed freeform micro-optics for optical coherence tomography fibre probes. Sci. Rep. 8:14789. [PubMed: 30287830]

[32]. Adams DC, Wang Y, Hariri LP and Suter MJ 2016 Advances in endoscopic optical coherence tomography catheter designs IEEE J. Sel Top. Quantum Electron 22 210–21

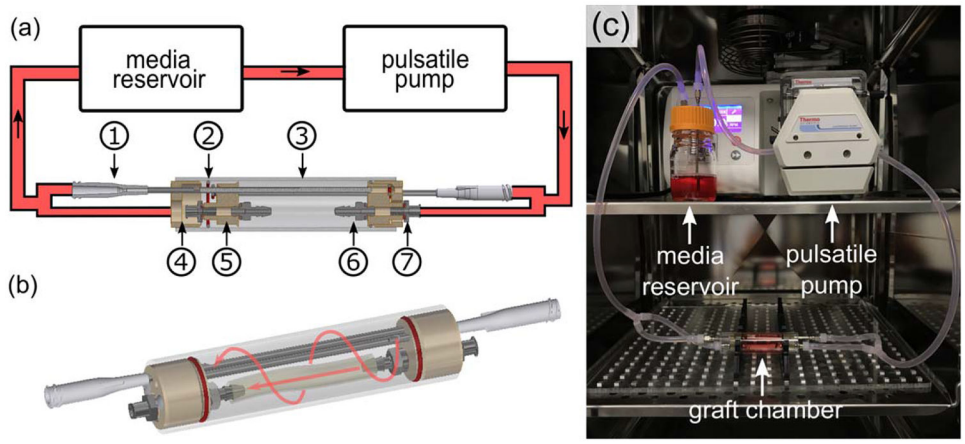

Figure 1.

Bioreactor. (a) Schematic of the bioreactor with a media reservoir, the pulsatile pump, and a custom graft chamber. The flow circulation direction is represented by the arrows in the tubes (in red). The graft chamber is composed of: ①stainless steel dispensing needle with distal end sealed by heat-curing epoxy, ②chmeical-resistant O-ring, ③Pyrex glass tubing, ④polysulfone inner flanges, ⑤polysulfone outer flanges, ⑥stainless steel straight connectors, ⑦stainless steel female luer. (b) Schematic of flow circulation inside the assembled graft chamber. One flow went through the intraluminal surface inside graft and the other circulates outside the graft. (c) Photograph of the bioreactor inside the incubator.

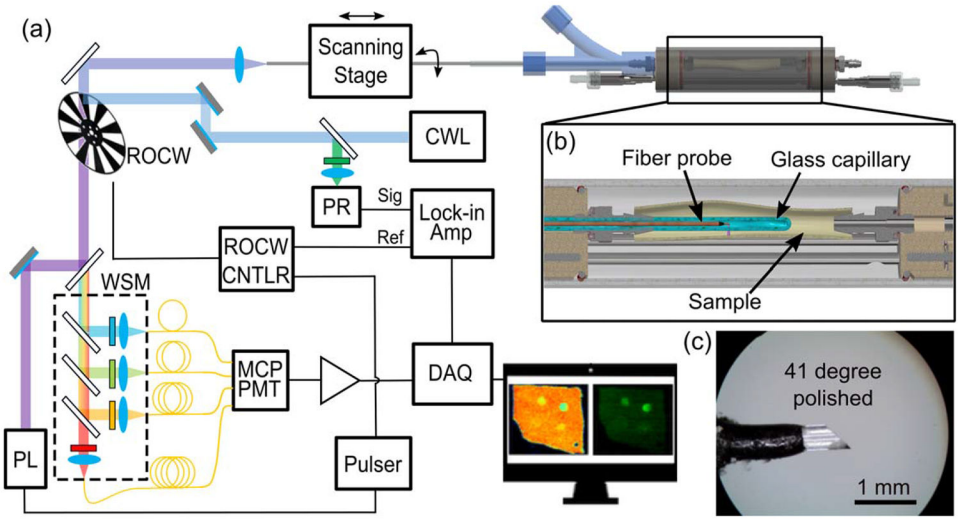

Figure 2.

Imaging setup. (a) Schematic of the endogenous and exogenous fluorescence system applied to luminal scanning inside the bioreactor graft chamber. PL: 355 nm pulsed laser; MCP-PMT: microchannel plate photomultiplier tube; WSM: wavelength selection module; ROCW: reflective optical chopper wheel; DAQ: digitizer; PR: photoreceiver; CWL: 440 nm continous-wave laser. (b) Cross section view of the graft chamber showing the side view fiber probe and the glass capillary used as imaging channel. (c) Microscope photograph showing the angle polished bessel probe.

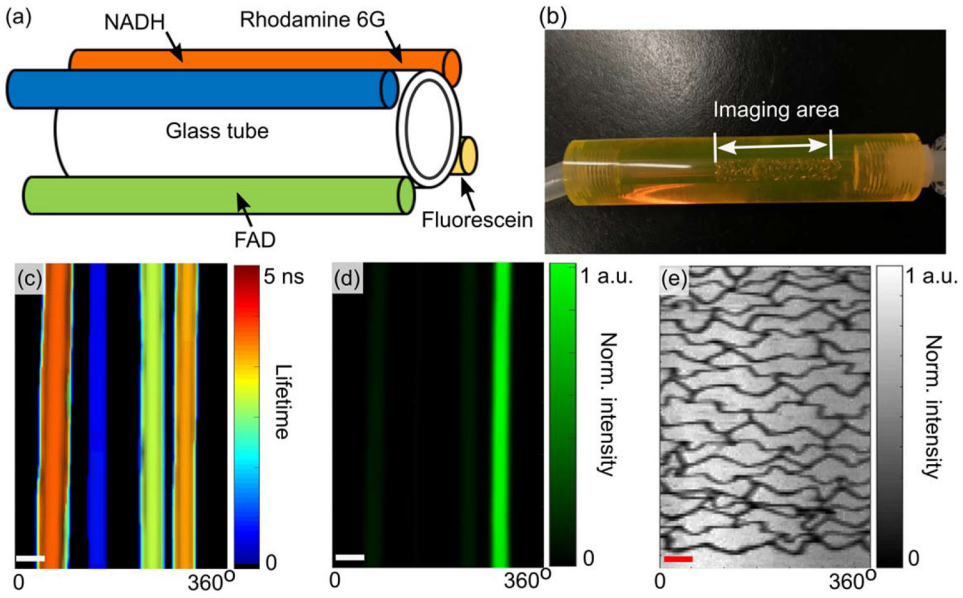

Figure 3.

Phantom imaging. (a) Schematic of the phantom. Four glass capillaries filled with Rhodamine 6G, NADH, FAD and Fluorescein were attached to the borosilicate tube, used as imaging channel. (b) Photograph of the stent phantom. (c) Intensity weighted lifetime image at SB3 (532–553 nm) of dye phantom. From left to right, the four columns represent Rhodamine 6G, NADH, FAD and Fluorescein. (d)Normalized eGFP fluorescence intensity image of dye phantom. Only fluorescein was visualized (e) normalized intensity image of the stent phantom at SB3. All three scale bars in (c)–(e) represent 2 mm.

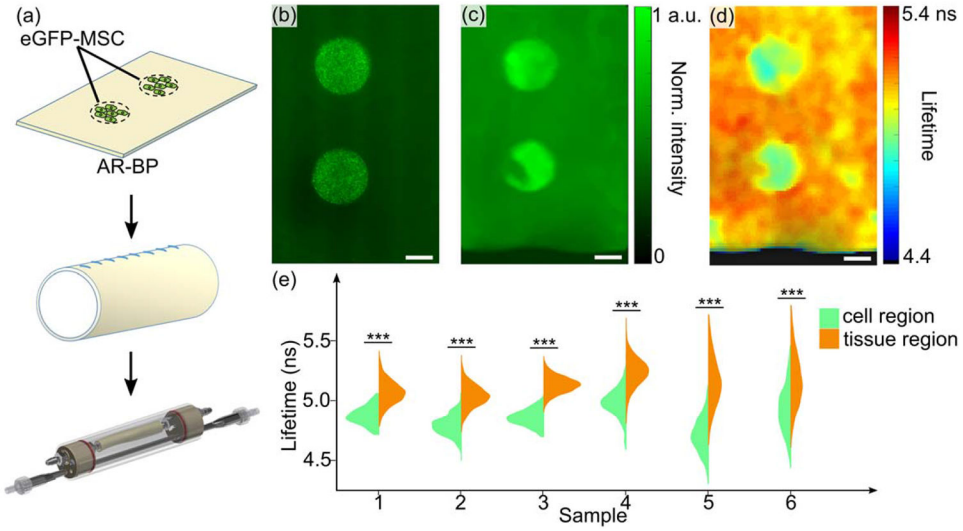

Figure 4.

Images of eGFP-hMSC seeded antigen removed bovine pericardium representative sample. (a) Schematic of sample preparation. (b) Fluorescence microscopy image of the flat sample before suturing. (c) Normalized eGFP fluorescence intensity intraluminal image of the same sample inside the bioreactor. (d) Corresponding intensity weighted fluorescence lifetime intraluminal image at SB3 (532–553 nm). (e) Split violin plot of SB3 lifetime distributions between cell and tissue regions for all six samples. The stars represent the statistical significance calculated with Student's t-test (*** $p<0.001$). All scale bars represent 2 mm.